

Quantum Criticality and Dynamical Kondo Effect in an $SU(2)$ Anderson Lattice Model

Haoyu Hu,^{1,*} Ang Cai,¹ and Qimiao Si^{1,†}

¹*Department of Physics and Astronomy, Rice Center for Quantum Materials, Rice University, Houston, Texas, 77005, USA*
(Dated: March 1, 2022)

Metallic quantum criticality often develops in strongly correlated systems with local effective degrees of freedom. In this work, we consider an Anderson lattice model with $SU(2)$ symmetry. The model is treated by the extended dynamical mean-field theory (EDMFT) in combination with a continuous-time quantum Monte Carlo method. We demonstrate a continuous quantum phase transition, establish the ensuing quantum critical point to be of a Kondo-destruction type, and determine the anomalous scaling properties. We connect the continuous nature of the transition to a dynamical Kondo effect, which we characterize in terms of a local entanglement entropy and related properties. This effect elucidates the unusual behavior of quantum critical heavy fermion systems.

Introduction. The nature of quantum critical points (QCPs), especially in metallic systems, is of extensive interest to a variety of strongly correlated systems[1–5]. Strong correlations often produce local effective degrees of freedom as a part of the building blocks for the low-energy physics. This is exemplified by antiferromagnetic (AFM) heavy fermion metals, in which local moments couple and interplay with itinerant electrons. The fate of the local moments and associated Kondo effect has played a central role in elucidating the AFM heavy fermion QCPs, both theoretically[6, 7] and experimentally[8–12]. Of particular importance is the notion of Kondo destruction[2], which corresponds to the disintegration of heavy quasiparticles. A Kondo-destruction QCP amounts to a delocalization-localization transition of the underlying f -electrons, thereby involving a sudden reconstruction of the Fermi surface. It also makes the quasiparticle weight at the QCP to vanish on the entire Fermi surface, which is responsible for the strange metal behavior in the quantum critical regime and the divergence of the effective carrier mass. Similar features may develop at the Mott transition and doped Mott insulators[13, 14], in light of the indications for a divergent carrier mass and a Fermi surface reconstruction in the high T_c cuprates near their optimal hole doping[15, 16].

The AFM quantum phase transitions in heavy fermion metals result from a competition between the Kondo and Ruderman-Kittel-Kasuya-Yosida (RKKY) couplings. These interactions respectively promote a Kondo-screened paramagnetic ground state and a long-range AFM order. Kondo destruction was initially studied by analyzing the fate of the Kondo effect near AFM QCPs [6, 17]. In the case of Ising-anisotropic Kondo lattice models, the continuous nature of the quantum phase transition has been demonstrated in a number of studies[18–21]. While some of the quantum critical heavy fermion systems are Ising-anisotropic[1, 9], others have a continuous spin symmetry[10–12, 22]. It is thus impor-

tant to address the issue in Kondo or Anderson lattice models with continuous spin symmetry. The latter is also important when connections are explored between the quantum criticality of the Kondo systems with that of the Mott-Hubbard systems such as the cuprates, which are to a good approximation $SU(2)$ symmetric.

In this Letter, we consider an Anderson lattice model with an $SU(2)$ symmetry. We study the lattice model in terms of a self-consistent Bose-Fermi Anderson model via the extended dynamical mean-field theory (EDMFT)[23–25]. Our study has become possible due to the recent development of a continuous-time Quantum Monte Carlo (CTQMC) approach suitable for the $SU(2)$ -symmetric Bose-Fermi Anderson model[26], which built on the general CTQMC method[27, 28]; importantly, we reach temperatures lower than 10^{-3} of the bare Kondo temperature. We show that the quantum phase transition is continuous. For the ensuing QCP, we demonstrate its Kondo-destruction nature, and find that the spin dynamics obey ω/T scaling. Equally important, we establish a dynamical Kondo effect by calculating the local entanglement entropy[29, 30] as well as the cross correlations between the local moment and conduction-electron spins. The dynamical Kondo effect underlies the continuous nature of the quantum phase transition, and elucidates the unusual properties of quantum critical heavy fermion systems.

Model and method. We study the Hamiltonian

$$H = (U/2) \sum_i \left[\sum_{\sigma} d_{i,\sigma}^{\dagger} d_{i,\sigma} - 1 \right]^2 + \sum_{ij} I_{ij} \mathbf{S}_i \cdot \mathbf{S}_j + V \sum_{i,\sigma} [c_{i,\sigma}^{\dagger} d_{i,\sigma} + d_{i,\sigma}^{\dagger} c_{i,\sigma}] + \sum_{p,\sigma} \epsilon_p c_{p,\sigma}^{\dagger} c_{p,\sigma}. \quad (1)$$

Here, $c_{i,\sigma}^{\dagger}$ ($d_{i,\sigma}^{\dagger}$) creates a conduction c (local d) electron of spin σ at site i , and $\mathbf{S}_i = (d_{i,\sigma}^{\dagger} \boldsymbol{\sigma} d_i)/2$ (with $\boldsymbol{\sigma}$ being the Pauli matrices) represents the spin of the d -electrons (denoting the physical f -electrons). The hybridization V couples the c -electrons, which has a dispersion ϵ_p , and

the d -electron spins, which involve an AFM RKKY interaction I_{ij} . Finally, the repulsive Hubbard interaction U is responsible for turning the d -electrons into local moments; when U is sufficiently large, the model is equivalent to a Kondo lattice Hamiltonian, with an effective AFM Kondo coupling J_K being second order in V .

The EDMFT approach[18, 23–25] takes into account the *dynamical* competition between the hybridization/Kondo and RKKY interactions. Here, the lattice Hamiltonian Eq. 1 is solved in terms of a self-consistent Bose-Fermi Anderson model. In the latter, the local d electrons couple to a fermionic bath and a bosonic bath, where the fermionic bath comes from the conduction electrons and the bosonic bath represents the fluctuations of local moments[31]. After integrating out both baths, we reach the following action:

$$\begin{aligned}
& S_{BFA} \\
&= \int_0^\beta d\tau \left[\sum_\sigma d_\sigma^\dagger \partial_\tau d_\sigma + \frac{U}{2} (n_{d,\uparrow} + n_{d,\downarrow} - 1)^2 + h_{loc} S^z \right] \\
&\quad - \int_0^\beta d\tau d\tau' \left[\sum_\sigma d_\sigma^\dagger(\tau) V^2 G_c(\tau - \tau') d_\sigma(\tau') \right. \\
&\quad \left. + (1/2) \sum_{\alpha \in \{x,y,z\}} S^\alpha(\tau) [\chi_0^\alpha]^{-1}(\tau - \tau') S^\alpha(\tau') \right], \quad (2)
\end{aligned}$$

where $\beta = 1/T$, h_{loc} is a static Weiss field, which captures the AFM order, while G_c and χ_0 denote the Green's functions of the fermionic and bosonic bath[31], respectively. The self-consistency conditions are:

$$\begin{aligned}
\chi_{loc}^\alpha(i\omega_n) &= \int_{-\infty}^{\infty} d\epsilon \rho_I(\epsilon) / [\epsilon + M^\alpha(i\omega_n)] \\
M^\alpha(i\omega_n) &= [\chi_0^\alpha]^{-1}(i\omega_n) + 1/\chi_{loc}^\alpha(i\omega_n) \\
G_c(i\omega_n) &= \int_{-\infty}^{\infty} d\epsilon \rho_0(\epsilon) / [-i\omega_n + \epsilon + \Sigma_c(i\omega_n)] \\
h_{loc} &= -[2I - [\chi_0^\alpha]^{-1}(i\omega_n = 0)] m_{AF}. \quad (3)
\end{aligned}$$

Here, $\alpha \in \{x, y, z\}$ represents the spin components, with the magnetic order taken along $\alpha = z$; $\rho_I(\epsilon)$ denotes the RKKY density of states, which is obtained from $\rho_I(\epsilon) = \sum_{\mathbf{q}} \delta(\epsilon - I_{\mathbf{q}})$. The RKKY interaction $I_{\mathbf{q}}$ is the Fourier transformation of I_{ij} , and is the most negative at the AFM wave vector \mathbf{Q} ; we consider $I_{\mathbf{Q}} = -2I$ and the density of states $\rho_I(\epsilon) = \theta(2I - |\epsilon|)/(4I)$, which incorporates two-dimensional magnetic fluctuations[6]. The irreducible (and momentum-independent) quantity $M^\alpha(i\omega_n)$ reflects a spin self-energy[23, 24]. The local irreducible spin susceptibility χ_{loc} and ordered moment m_{AF} are:

$$\begin{aligned}
\chi_{loc}^\alpha(\tau) &= \langle T_\tau : S^\alpha : (\tau) : S^\alpha : (0) \rangle_{S_{BFA}} \\
m_{AF} &= \langle S^z \rangle_{S_{BFA}}. \quad (4)
\end{aligned}$$

The expectation value $\langle \dots \rangle_{S_{BFA}}$ is taken with respect to the action S_{BFA} (Eq. 2), and the normal-ordered operators are $: S^z : \equiv S^z - \langle S^z \rangle_{S_{BFA}}$ and $: S^{x,y} : \equiv S^{x,y}$. We

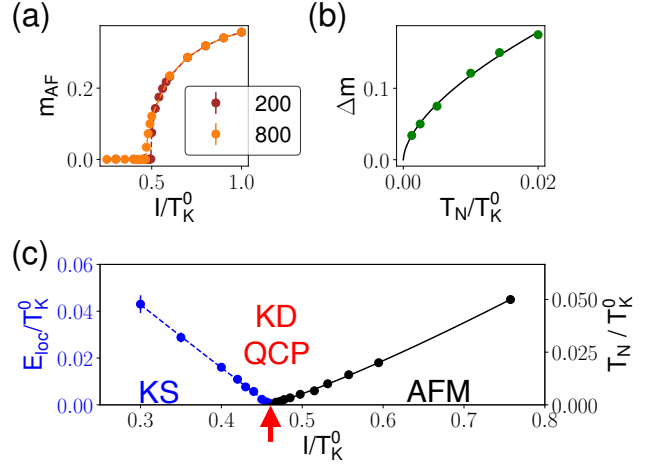


FIG. 1: (Color online) (a) Evolution of the AFM order parameter m_{AF} with the ratio I/T_K^0 , at inverse temperatures $\beta T_K^0 = 200, 800$. (b) Jump in the order parameter Δm vs. the Néel temperature T_N , extrapolating to zero as $T_N \rightarrow 0^+$. (c) Phase diagram, showing also the Kondo-destruction (KD) energy scale E_{loc}^* vs. I/T_K^0 . KS and AFM respectively denote Kondo-screened and antiferromagnetic phases. The red arrow marks the QCP at $I = I_c$.

consider a generic electron filling[32] with the conduction-electron band having a nonzero density of states at the zero energy in terms of a featureless $\rho_0(\epsilon)$, for which $G_c(i\omega_n) = \frac{1}{2D} \log(\frac{-i\omega_n + D}{-i\omega_n - D})$. The equations are iterated until convergence, which corresponds to the differences between the two iterations being less than 0.1%.

Continuous AFM quantum phase transition. To determine the phase diagram, we work with the generic parameters $U = 0.25, V = 0.40, D = 1.0$, for which the bare Kondo temperature $T_K^0 = 1$. Hereinafter, we only vary the RKKY interaction I to tune the ratio of the RKKY interaction to the bare Kondo scale, I/T_K^0 .

We perform calculations at various values of temperature T and the tuning parameter I/T_K^0 . For a given T , an isothermal AFM phase transition is seen through the onset of the order parameter m_{AF} , as illustrated in Fig. 1(a). We observe a jump in the order parameter, Δm , at the isothermal transition point, indicating that the finite-temperature phase transition is first order[19]. The phase diagram is shown in Fig. 1(c). As we approach the zero-temperature phase transition along the T_N line (black solid curve), Δm decreases as shown in Fig. 1(b); within the error bar, it extrapolates to zero in the zero temperature limit. This establishes a continuous quantum phase transition at $I = I_c$.

Kondo destruction, quantum criticality and anomalous scaling. We now turn to the nature and properties of the QCP. We focus on the $\alpha = z$ component of the spin susceptibility, which captures the AFM order and, outside of the ordered region, is equal to the other two

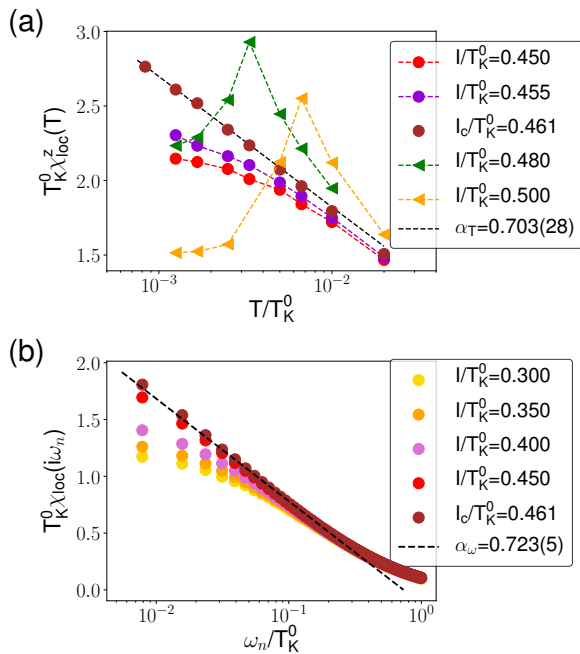


FIG. 2: (Color online) (a) Temperature dependence of the local spin susceptibility $T_K^0 \chi_{loc}^z(T)$. The QCP is at $I_c/T_K^0 = 0.461$ (see Fig. S2[31]). (b) The dynamical local spin susceptibility in the paramagnetic phase ($I \leq I_c$) at inverse temperature $\beta T_K^0 = 800$.

components: we will use χ^z to denote this quantity inside of the AFM order and simply χ outside of it.

The temperature dependence of the static local spin susceptibility $\chi_{loc}(T)$, defined as $\chi_{loc}(i\omega_n = 0, T)$, is presented in Fig. 2(a) (as well as Fig. S1[31]) for various values of the RKKY interaction I . For $I > I_c$, it shows a peak at T_N . For $I < I_c$, it saturates to a finite value at low temperatures, signifying Kondo screening. $\chi_{loc}(T \rightarrow 0)$ is divergent at $I = I_c$, the QCP. This means that, at the AFM QCP, the Kondo effect is placed at the critical Kondo-destruction point, as seen from the renormalization-group (RG) flow of the Bose-Fermi Kondo model[23, 33–36] (summarized in supplementary materials[31], Fig. S2; particularly the dashed arrow). More precisely, $\chi_{loc}(T)$ at the QCP is logarithmically singular, corresponding to the bosonic bath of the Bose-Fermi Anderson model having a sub-ohmic spectrum with its power-law exponent 0^+ (Ref. [6]). We can then express $\chi_{loc}(T)$ in the following form [17]:

$$\chi_{loc}(T) = -\frac{\alpha_T}{4I} \log(T) + b_T. \quad (5)$$

In Fig. 2(b), we show the dynamical local spin susceptibility $\chi_{loc}(i\omega_n)$ in the paramagnetic part of the phase diagram. At the critical point, $I = I_c$, it also is found to be singular and satisfy

$$\chi_{loc}(i\omega_n) = -\frac{\alpha_\omega}{4I} \log(\omega_n) + b_\omega \quad (6)$$

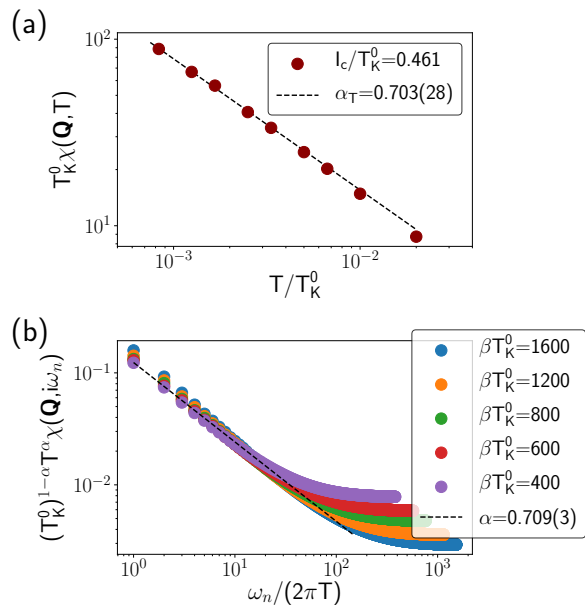


FIG. 3: (Color online) (a) Static lattice spin susceptibility vs. temperature at $I = I_c$. (b) Demonstration of ω_n/T scaling for the dynamical lattice spin susceptibility at $I = I_c$.

in a large dynamical range ($0.004T_K^0 \leq \omega_n \lesssim 0.300T_K^0$). Away from the critical point, $I > I_c$, the local susceptibility saturates, which places the local Kondo problem to be on the Kondo-screened side of the RG flow (supplementary materials[31], Fig. S2). We can introduce a local Kondo energy scale E_{loc}^* to characterize this saturation[19, 37], by fitting $\chi_{loc}(i\omega_n)$ in terms of $A + B \log(\omega_n + E_{loc}^*)$. The resulting E_{loc}^* as a function of the tuning parameter I/T_K^0 is already shown in Fig. 1(c). This energy scale collapses as the system approaches the QCP, manifesting the Kondo destruction at the QCP.

These results also imply that, at the QCP, $I = I_c$, the AFM spin susceptibility has the following power-law temperature and frequency dependences[31]:

$$\begin{aligned} \chi(\mathbf{Q}, T) &\propto T^{-\alpha_T}, \\ \chi(\mathbf{Q}, i\omega_n) &\propto \omega_n^{-\alpha_\omega}. \end{aligned} \quad (7)$$

The static lattice susceptibility $\chi(\mathbf{Q}, T)$ is shown in Fig. 3(a), and its dynamical counterpart, at a low-temperature $T = 1.125 \times 10^{-3} T_K^0$, is presented in Fig. S3. We find the critical exponents to be $\alpha_T = 0.701(28)$ and $\alpha_\omega = 0.723(5)$.

The temperature and frequency exponents have the same fractional value within the numerical uncertainty. This result suggests that the AFM dynamical spin susceptibility obeys ω/T scaling in the quantum critical regime. To address this issue further, we calculate the AFM dynamical spin susceptibility at the QCP, $I = I_c$, as a function of both frequency and temperature over a range of low temperatures ($T_K^0/1600 < T < T_K^0/400$). In Fig. 3(b), we show that $(T_K^0)^{1-\alpha} T^\alpha \chi(\mathbf{Q}, \omega_n, T)$ at the

various temperatures collapses in the form of ω_n/T scaling. The critical exponent $\tilde{\alpha}$ is unbiasedly determined by this procedure. Its value, $\alpha = 0.709(3)$, is compatible with α_T and α_ω described earlier. Together, these results demonstrate that the dynamical spin susceptibility displays ω/T scaling and fractional scaling exponents.

The usual spin-density-wave QCP[38–40] falls within the Landau framework of order-parameter fluctuations and corresponds to a Gaussian fixed point. The ω/T scaling we found signifies an interacting fixed point. The collapse of the energy scale E_{loc}^* at the QCP signifies that the Kondo destruction underlies the beyond-Landau physics. In turn, this implies that the quasiparticle weight vanishes as the QCP is approached, and the Fermi surface jumps between large (counting the Kondo resonance) and small (not counting the Kondo resonance) across the QCP.

Dynamical Kondo effect. We now turn to understand why the quantum phase transition is continuous when the heavy quasiparticles disintegrate at the transition. To do so, we first calculate the entanglement entropy of a local d electron. The entanglement property has been calculated in the standing-alone Bose-Fermi Kondo impurity models[29, 30], but has not been studied in any Kondo/Anderson lattice models. The local entanglement entropy is defined as $S_{e,loc} = -\text{Tr}[\rho_{loc} \log(\rho_{loc})]$, where ρ_{loc} is the density matrix of the local d electron[41]. In Fig. 4(a), we show the evolution of $S_{e,loc}$ across the QCP. In the Kondo-screened phase, due to the Kondo effect, the local d electrons and the conduction-electron band are Kondo entangled, which results in a large $S_{e,loc}$ [we find $S_{e,loc}(I=0) = 1.386$]. Increasing the RKKY interaction I through the QCP, I_c , $S_{e,loc}$ drops precipitously, capturing the Kondo destruction. Importantly, it stays nonzero inside the Kondo-destroyed phase at $I > I_c$. This implies that residual Kondo-singlet correlations persist. This is to be contrasted with the naive mean-field picture, which would have associated the Kondo destruction with a complete decoupling between the local d electron and conduction-electron bands; in that picture, the entanglement entropy must vanish. We interpret our result as signifying the persistence of the dynamical Kondo-singlet correlations in the Kondo-destroyed phase, even though the static Kondo-singlet amplitude has vanished in the ground state.

This point can be further demonstrated by the cross correlation between the local moment and conduction-electron spins, which has recently been considered in quantum impurity models[42]. The expectation value of $\langle S^z s_c^z \rangle$ is shown in Fig. 4 (b). While it is naturally nonzero in the Kondo-screened phase at $I < I_c$, it remains so at the Kondo-destruction QCP ($I = I_c$) and in the Kondo-destroyed phase ($I > I_c$). Through Kramers-Kronig relation[42], our result, derived for the first time in any lattice model, implies the persistence of the dynamical Kondo correlations across the QCP and into the

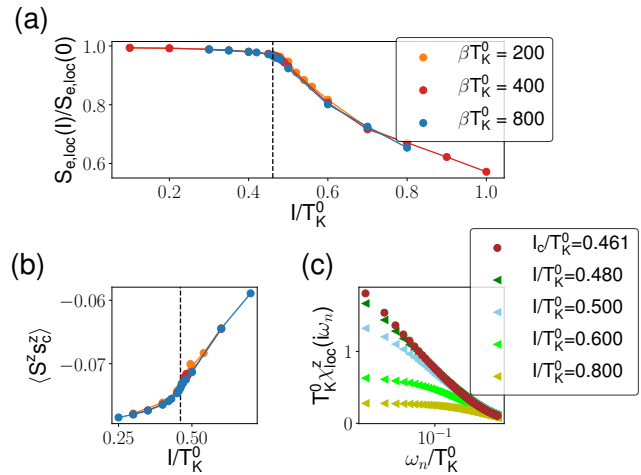


FIG. 4: (Color online) (a) Evolution of the local entanglement entropy with the tuning parameter I/T_K^0 . The vertical dashed line marks the AFM QCP. (b) $\langle S^z s_c^z \rangle$ vs. the tuning parameter across the QCP. (c) Dynamical local susceptibility for $I \geq I_c$ and $\beta T_K^0 = 800$.

Kondo-destroyed phase.

The dynamical Kondo effect can be further illustrated by the irreducible local spin susceptibility, $\chi_{loc}(i\omega_n)$, in the ordered phase. The result is given in Fig. 4 (c). If the local d electrons were completely decoupled from the conduction-electron band, $\chi_{loc}(i\omega_n)$ would vanish at nonzero frequencies. Indeed, $\chi_{loc}(i\omega_n)$ is negligible at $I \gg I_c$, *i.e.* deep into the ordered phase. As I is reduced towards I_c , $\chi_{loc}(i\omega_n)$ progressively grows, reflecting the increased dynamical Kondo-singlet correlations in the Kondo-destroyed phase.

The vanishing of the spectral weight for the well-defined Kondo resonance as the transition is approached from the paramagnetic side underlies the sudden jump of the Fermi surface across the QCP. In a naive mean-field picture, one would have expected the transition to be first order. The dynamical Kondo effect we have demonstrated underlies the continuity of the Kondo correlations across the transition and into the Kondo-destroyed phase, which makes possible for the quantum phase transition to be continuous.

Discussion. Several remarks are in order. First, the dynamical Kondo effect captures the quantum fluctuations in the Kondo-destroyed phase. One of the unusual properties observed[43, 44] in the prototype heavy fermion metals with Kondo-destruction QCPs is the pronounced quasiparticle mass in the Kondo-destroyed phase. The quantum fluctuations associated with the dynamical Kondo effect provide a natural understanding of this property.

Second, our EDMFT-based results for the beyond-Landau QCP in the $SU(2)$ Anderson lattice model set the stage to connect with what happens in the $SU(2)$

Hubbard-Heisenberg models. Recently, EDMFT analyses have also been carried out in the latter models[45–47], and have implicated related QCPs. Since the effective local problem in that case is quite similar to what we analyze for the $SU(2)$ Anderson lattice model, it will be instructive to see whether any effect analogous to the dynamical Kondo effect underlies the (nearly) continuous nature of the quantum phase transitions in those models.

Summary. The $SU(2)$ -symmetric Anderson lattice model has been studied using the EDMFT method, and is shown to display a continuous AFM quantum phase transition. We have established the Kondo-destruction nature of the QCP, demonstrated that the spin dynamics obey ω/T scaling and found fractional temperature and frequency exponents. Finally, we have reported the first calculation of the local entanglement entropy across the Kondo-destruction QCP in any Anderson/Kondo lattice model. The result implies a dynamical Kondo effect, which is crucial for realizing the continuous nature of the quantum phase transition and for elucidating the unusual properties of the quantum critical heavy fermion systems. As such, our results considerably deepen the understanding of quantum critical heavy fermion metals with continuous spin symmetry, and set the stage to link the beyond-Landau quantum criticality of heavy fermion systems with its counterpart in Mott-Hubbard systems.

We thank Kevin Ingersent, Stefan Kirchner, Chia-Chuan Liu, Silke Paschen, Jed Pixley, and Frank Steglich for useful discussions. The work was in part supported by the NSF (DMR-1920740) and the Robert A. Welch Foundation (C-1411). Computing resources were supported in part by the Data Analysis and Visualization Cyberinfrastructure funded by NSF under grant OCI-0959097 and an IBM Shared University Research (SUR) Award at Rice University, and by the Extreme Science and Engineering Discovery Environment (XSEDE) by NSF under Grants No. DMR170109. Q.S. acknowledges the hospitality of the Aspen Center for Physics (NSF, PHY-1607611).

* Electronic address: hh25@rice.edu

† Electronic address: qmsi@rice.edu

- [1] Special issue: Quantum Phase Transitions, *J. Low Temp. Phys.* **161**, 1 (2010).
- [2] S. Kirchner, S. Paschen, Q. Chen, S. Wirth, D. Feng, J. D. Thompson, and Q. Si, *Rev. Mod. Phys.* **92**, 011002 (2020).
- [3] B. Keimer and J. E. Moore, *Nat. Phys.* **13**, 1045 (2017).
- [4] P. Coleman and A. J. Schofield, *Nature* **433**, 226 (2005).
- [5] S. Sachdev, *Quantum Phase Transitions* (Cambridge University Press, Cambridge, 1999).
- [6] Q. Si, S. Rabello, K. Ingersent, and J. Smith, *Nature* **413**, 804 (2001).
- [7] P. Coleman, C. Pépin, Q. Si, and R. Ramazashvili, *J. Phys. Cond. Matt.* **13**, R723 (2001).
- [8] L. Prochaska, X. Li, D. C. MacFarland, A. M. Andrews, M. Bonta, E. F. Bianco, S. Yazdi, W. Schrenk, H. Detz, A. Limbeck, et al., *Science* **367**, 285 (2020).
- [9] A. Schröder, G. Aeppli, R. Coldea, M. Adams, O. Stockert, H. v. Löhneysen, E. Bucher, R. Ramazashvili, and P. Coleman, *Nature* **407**, 351 (2000).
- [10] S. Paschen, T. Lühmann, S. Wirth, P. Gegenwart, O. Trovarelli, C. Geibel, F. Steglich, P. Coleman, and Q. Si, *Nature* **432**, 881 (2004).
- [11] H. Shishido, R. Settai, H. Harima, and Y. Ōnuki, *J. Phys. Soc. Jpn.* **74**, 1103 (2005).
- [12] T. Park, F. Ronning, H. Q. Yuan, M. B. Salamon, R. Movshovich, J. L. Sarrao, and J. D. Thompson, *Nature* **440**, 65 (2006).
- [13] T. Senthil, *Phys. Rev. B* **78**, 035103 (2008).
- [14] H. Terletska, J. Vučićević, D. Tanasković, and V. Dobrosavljević, *Phys. Rev. Lett.* **107**, 026401 (2011).
- [15] B. J. Ramshaw, S. E. Sebastian, R. D. McDonald, J. Day, B. S. Tan, Z. Zhu, J. B. Betts, R. Liang, D. A. Bonn, W. N. Hardy, et al., *Science* **348**, 317 (2015).
- [16] S. Badoux, W. Tabis, F. Laliberté, G. . Grissonnanche, B. Vignolle, D. Vignolles, J. Béard, D. A. Bonn, W. N. Hardy, R. Liang, et al., *Nature* **531**, 210 (2016).
- [17] Q. Si, S. Rabello, K. Ingersent, and J. L. Smith, *Phys. Rev. B* **68**, 115103 (2003).
- [18] Q. Si, J. H. Pixley, E. Nica, S. J. Yamamoto, P. Goswami, R. Yu, and S. Kirchner, *Journal of the Physical Society of Japan* **83**, 061005 (2014).
- [19] J.-X. Zhu, D. R. Grempel, and Q. Si, *Phys. Rev. Lett.* **91**, 156404 (2003).
- [20] M. T. Glossop and K. Ingersent, *Phys. Rev. Lett.* **99**, 227203 (2007).
- [21] J.-X. Zhu, S. Kirchner, R. Bulla, and Q. Si, *Phys. Rev. Lett.* **99**, 227204 (2007).
- [22] P. Das, S.-Z. Lin, N. J. Ghimire, K. Huang, F. Ronning, E. D. Bauer, J. D. Thompson, C. D. Batista, G. Ehlers, and M. Janoschek, *Phys. Rev. Lett.* **113**, 246403 (2014).
- [23] Q. Si and J. L. Smith, *Phys. Rev. Lett.* **77**, 3391 (1996).
- [24] J. L. Smith and Q. Si, *Phys. Rev. B* **61**, 5184 (2000).
- [25] R. Chitra and G. Kotliar, *Phys. Rev. Lett.* **84**, 3678 (2000).
- [26] A. Cai and Q. Si, *Phys. Rev. B* **100**, 014439 (2019).
- [27] E. Gull, A. J. Millis, A. I. Lichtenstein, A. N. Rubtsov, M. Troyer, and P. Werner, *Rev. Mod. Phys.* **83**, 349 (2011).
- [28] J. Otsuki, *Phys. Rev. B* **87**, 125102 (2013).
- [29] J. H. Pixley, T. Chowdhury, M. T. Mieczkowski, J. Stephens, C. Wagner, and K. Ingersent, *Phys. Rev. B* **91**, 245122 (2015).
- [30] C. Wagner, T. Chowdhury, J. H. Pixley, and K. Ingersent, *Phys. Rev. Lett.* **121**, 147602 (2018).
- [31] Supplemental material.
- [32] Q. Si, J.-X. Zhu, and D. R. Grempel, *Journal of Physics: Condensed Matter* **17**, R1025 (2005).
- [33] J. L. Smith and Q. Si, *Europhysics Letters (EPL)* **45**, 228 (1999).
- [34] A. M. Sengupta, *Phys. Rev. B* **61**, 4041 (2000).
- [35] L. Zhu and Q. Si, *Phys. Rev. B* **66**, 024426 (2002).
- [36] G. Zaránd and E. Demler, *Phys. Rev. B* **66**, 024427 (2002).
- [37] D. Grempel and Q. Si, *Phys. Rev. Lett.* **91**, 026401 (2003).
- [38] J. A. Hertz, *Phys. Rev. B* **14**, 1165 (1976).
- [39] A. Millis, *Phys. Rev. B* **48**, 7183 (1993).
- [40] T. Moriya, Spin fluctuations in itinerant electron magnetism,

- vol. 56 (Springer Science & Business Media, 2012).
- [41] D. Larsson and H. Johannesson, *Phys. Rev. A* **73**, 042320 (2006).
- [42] A. Cai, H. Hu, K. Ingersent, S. Paschen, and Q. Si, arXiv:1904.11471 (2019).
- [43] V. Martelli, A. Cai, E. M. Nica, M. Taupin, A. Prokofiev, C.-C. Liu, H.-H. Lai, R. Yu, K. Ingersent, R. Kuchler, et al., *Proceedings of the National Academy of Sciences* **116**, 17701 (2019).
- [44] P. Gegenwart, J. Custers, C. Geibel, K. Neumaier, T. Tayama, K. Tenya, O. Trovarelli, and F. Steglich, *Phys. Rev. Lett.* **89**, 056402 (2002).
- [45] D. Joshi, C. Li, G. Tarnopolsky, A. Georges, and S. Sachdev, arXiv:1912.08822 (2020).
- [46] P. Cha, N. Wentzell, O. Parcollet, A. Georges, and E. Kim, arXiv:2002.07181 (2020).
- [47] G. Tarnopolsky, C. Li, D. Joshi, and S. Sachdev, arXiv:2002.12381 (2020).

Supplementary Material

EXTENDED DYNAMICAL MEAN FIELD THEORY

The EDMFT approach treats the Anderson lattice model, Eq. (1) of the main text, in terms of a Bose-Fermi Anderson model:

$$\begin{aligned}
 H &= H_{loc} + H_B + H_F \\
 H_{loc} &= \frac{U}{2}(n_{d,\uparrow} + n_{d,\downarrow} - 1)^2 + h_{loc} S^z \\
 H_B &= \sum_p \omega_p \phi_p^\dagger \cdot \phi_p + g \sum_p \mathbf{S} \cdot (\phi_p^\dagger + \phi_{-p}) \\
 H_F &= \sum_{p,\sigma} E_p c_{p,\sigma}^\dagger c_{p,\sigma} + V \sum_{p,\sigma} (c_{p,\sigma}^\dagger d_\sigma + d_\sigma^\dagger c_{p,\sigma}).
 \end{aligned} \tag{S.1}$$

Here, $n_{d,\sigma} = d_\sigma^\dagger d_\sigma$, and $c_{p,\sigma}$ describes the fermionic bath with dispersion E_p . In addition, ϕ_p represents a three-component bosonic bath, with dispersion ω_p ; it captures the fluctuations of the local moments. Integrating out the ϕ bosons and c fermions leads to the action given in Eq. 2 of the main text.

IDENTIFYING THE QUANTUM CRITICAL POINT

We identify the critical point through two complementary procedures. One is the extrapolation of the $T_N(I)$ curve to zero temperature. Another is to examine the behavior of the static local susceptibility. As we discussed in the main text, the static local susceptibility has different behavior in different phases. In the Kondo-screened phase, $\chi_{loc}^z(T)$ saturates when we lower the temperature T towards zero. In the AFM phase, as we lower the temperature, $\chi_{loc}^z(T)$ first goes upwards, which corresponds to the Curie-Weiss behavior. It then drops off upon the onset of the AFM order. Based on this insight, we can search for the critical RKKY interaction I_c (as mentioned in the main text, the

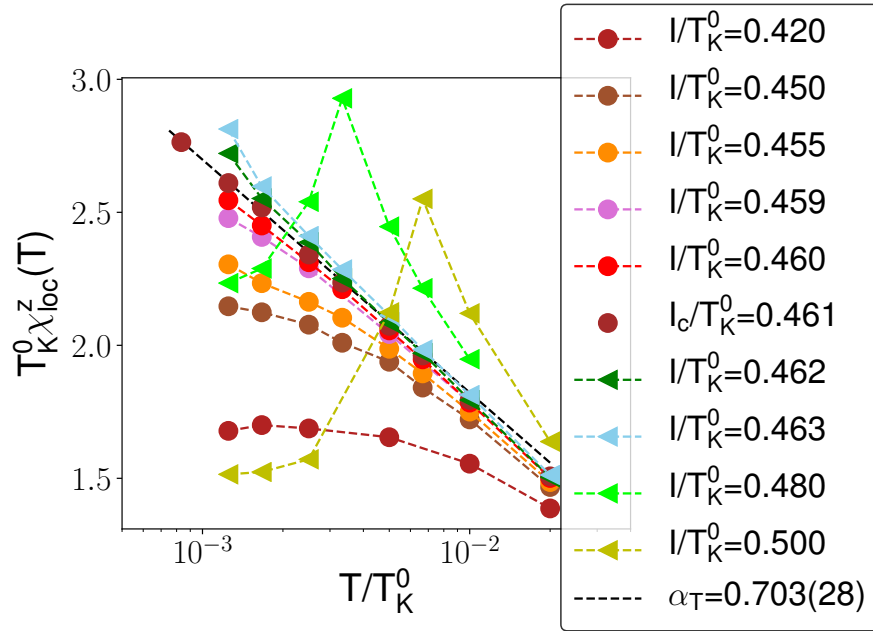


FIG. S1: (Color online) Static local susceptibility as a function of temperature, for a dense set of RKKY interactions I .

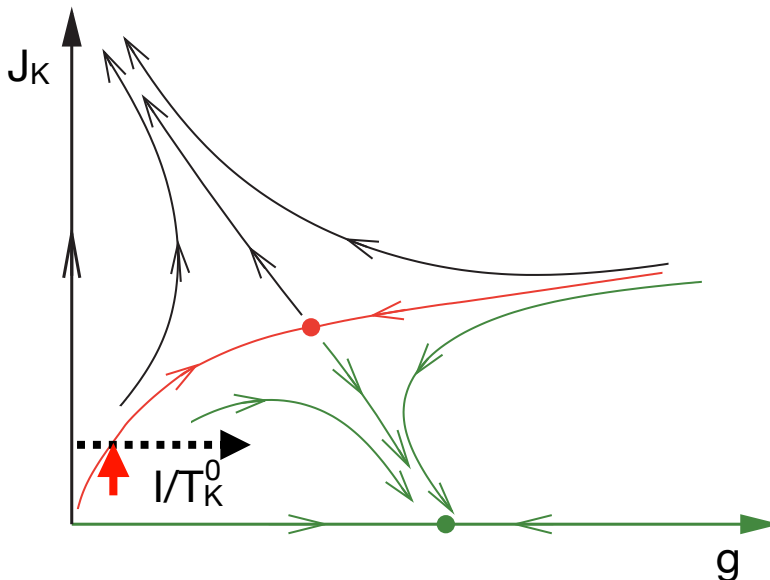


FIG. S2: (Color online) RG flow of the Bose-Fermi Kondo/Anderson model [1]. g is the coupling between the local moment and bosonic bath, and J_K is the Kondo coupling between the local moment and fermionic bath.

bare Kondo scale is fixed) by the point where the singular (logarithmic) behavior survives to the lowest temperature. We show the evolution of $\chi_{loc}^z(T)$ at different ratios of I/T_K^0 in Fig. S1. At $I = I_c = 0.461T_K^0$, $\chi_{loc}^z(T)$ has the most straight-line behavior in the semi-log plot.

KONDO DESTRUCTION AND THE RENORMALIZATION GROUP FLOW OF THE BOSE-FERMI KONDO MODEL

In Fig. S2, we show the renormalization group (RG) flow of the effective Bose-Fermi Kondo model [1], where g denotes the coupling constant between the local moment and bosonic bath, and J_K represents the Kondo coupling. In our study of the Anderson lattice model, we fixed the bare Kondo temperature T_K^0 and tune the RKKY interaction I . For the corresponding Bose-Fermi impurity model, this is illustrated by the dashed arrow in Fig. S2. The model may flow to three fixed points by tuning I/T_K^0 . For small I/T_K^0 , the impurity model flows to a Kondo-screened fixed point. For large I/T_K^0 , the model flows to a Kondo-destroyed fixed point with zero J_K . In between, the system passes through the separatrix (the red arrow in Fig. S2), where it flows to the Kondo-destruction QCP. On the separatrix, *e.g.* upon reaching the red arrow following the dashed line from left in Fig. S2, the local spin susceptibility $\chi_{loc}(T \rightarrow 0)$ diverges. The observations from the RG flow are consistent with the results presented in the main text.

RELATION BETWEEN THE LOCAL SUSCEPTIBILITY AND ANTIFERROMAGNETIC LATTICE SUSCEPTIBILITY

In this section, we summarize the calculation of the antiferromagnetic lattice susceptibility, which in the paramagnetic phase is determined by the Dyson equation[2, 3]:

$$\chi^\alpha(\mathbf{q}, i\omega_n) = \langle S^\alpha(\mathbf{q}, i\omega_n) S^\alpha(\mathbf{q}, -i\omega_n) \rangle = 1/[M^\alpha(i\omega_n) + I_{\mathbf{q}}] , \quad (\text{S.2})$$

with $\alpha \in \{x, y, z\}$. At the antiferromagnetic wave vector \mathbf{Q} , we have

$$\chi^\alpha(\mathbf{Q}, i\omega_n) = 1/[M^\alpha(i\omega_n) - 2I] . \quad (\text{S.3})$$

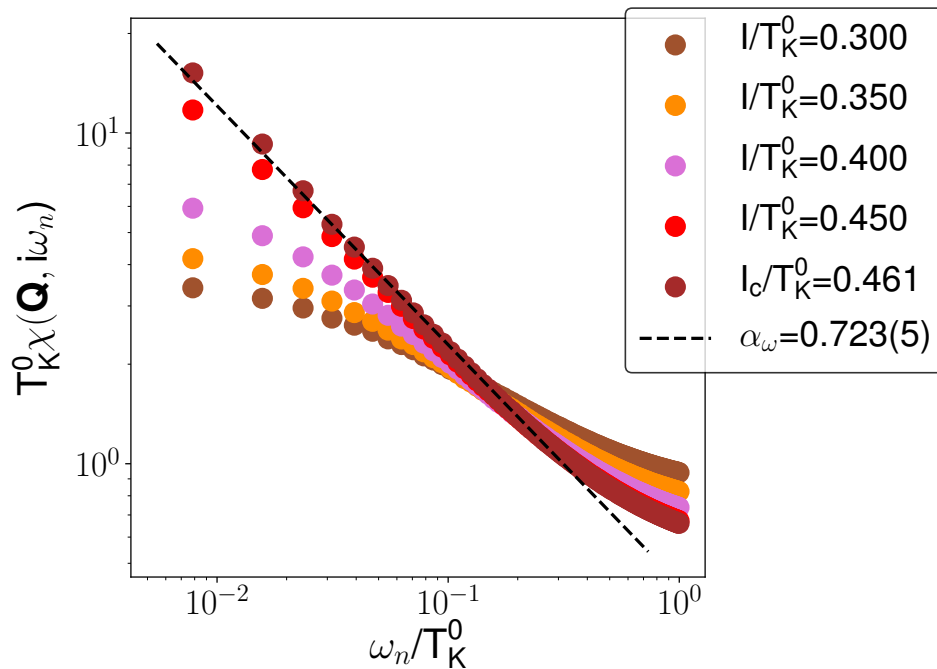


FIG. S3: (Color online) Frequency dependence of the antiferromagnetic lattice spin susceptibility at the inverse temperature $\beta T_K^0 = 800$

Combining the above equation with the self-consistent equations in the main text, we can derive the following asymptotic relation between $\chi_{loc}(i\omega_n)$ and $\chi(\mathbf{Q}, i\omega_n)$, which is valid in the region of $4I\chi_{loc}(i\omega_n) \gg 1$

$$\begin{aligned} \chi^\alpha(\mathbf{Q}, i\omega_n) &= \frac{1}{4I} [\exp(4I\chi_{loc}^\alpha(i\omega_n)) - 1] \\ &\approx \frac{\exp(4I\chi_{loc}^\alpha(i\omega_n))}{4I} \end{aligned} \quad (\text{S.4})$$

FREQUENCY DEPENDENCE OF THE ANTIFERROMAGNETIC DYNAMICAL SPIN SUSCEPTIBILITY

In Fig. S3, we show the frequency dependence of the antiferromagnetic lattice spin susceptibility upon approaching the QCP from the paramagnetic phase. At the QCP with $I = I_c$, according to the relationship between local and lattice susceptibilities (Eq. S.4), the antiferromagnetic lattice susceptibility follows a power-law behavior with $\chi(\mathbf{Q}, i\omega_n) \sim \omega_n^{-\alpha_\omega}$. Away from the QCP with $I < I_c$, it saturates at low frequencies; this reflects the effect of a nonzero static Kondo singlet amplitude in the ground state.

-
- [1] L. Zhu and Q. Si, Phys. Rev. B **66**, 024426 (2002).
 [2] Q. Si and J. L. Smith, Phys. Rev. Lett. **77**, 3391 (1996).
 [3] J. L. Smith and Q. Si, Phys. Rev. B **61**, 5184 (2000).